Proceedings of the 25th International Conference on
Port and Ocean Engineering under Arctic Conditions
June 9-13, 2019, Delft, The Netherlands

Non-smooth DEM Simulation for Interaction of Conical Structure and Managed Ice Floes using Breakable Ice Element

Kenta Hasegawa[1], Shotaro Uto[1], Haruhito Shimoda[1], Daisuke Wako[1], Takatoshi Matsuzawa[1]
[1] National Maritime Research Institute, National Institute of Maritime, Port and Aviation Technology, Tokyo, Japan

ABSTRACT

To estimate global ice loads exerted on a structure due to interaction with managed ice floes, we have been developing a numerical simulation method by a non-smooth discrete element method. In this study, a breakable ice element consisting of small square rigid body with a fixed joint function of the physics engine is introduced to our numerical simulation method in order to represent ice failure. To clarify the effect of the ice failure, we compared simulation results with experimental results obtained from ice tank tests conducted in National Maritime Research Institute. The results show that the breakable ice elements reasonably reduce peak loads to the experimental results in the condition where peak loads became extremely high in the simulation not considering ice failure. Furthermore, it is found that the state of ice failure is different depending on a coefficient of friction between ice floes. The state of ice failure similar to the experiment was sometimes observed for a larger coefficient of friction between ice floes.

KEY WORDS: Managed ice loads; Failure; Non-smooth DEM; Physics engine; Ice tank test.

INTRODUCTION

The United States Geological Survey has reported that about 13% of the world's undiscovered oil and 30% of the world's undiscovered gas may be found in the area north of the Arctic Circle (Gautier and Moore, 2017). It is also mentioned that sea ice has been declining in the Arctic sea, where oil and gas development is expected. Arctic resource development, however, suffers great threat from sea ice and iceberg. In the case of using a floating structure such as a drilling rig at sites where sea ice exists ice management, an operation to break sea ice into smaller pieces by icebreakers, is carried out in order to reduce the ice load and improve the station keeping ability.

Managed ice floes collide with the structure or other floes resulting in horizontal and/or vertical displacement and in some cases global ice failure such as bending or splitting occurs. To numerically simulate such managed ice floes-structure interaction, it is necessary to deal with multiple body problems. Discrete Element Methods (DEMs) are often used for these problems in many fields. In ice engineering, for example, Polojärvi et al. (2012) have conducted and

simulated laboratory scale punch through tests on floating rubble consisting of plastic blocks with a 3D discrete numerical model. Konno et al. (2013) have numerically reproduced brash ice channel experiments with more than 10^4 ice pieces by using the Open Dynamics Engine (ODE). Dudal et al. (2015) show their simulator for offshore structure and ice sheet interaction. In the simulator, the collision and dynamic of objects and the influence of water currents are simulated by the Bullet Physics Library (Bullet) and CFD OpenFOAM software, and the bending failure and the crushing ice failure are based on the model of Nevel in 1992 and Daley in 1991, respectively. Lubbad and Løset (2015) have developed a simulator dealing with the interaction between managed ice and floating structures by DEM with analytical closed form solutions to represent the icebreaking processes. However, there are few literatures comparing ice loads, behavior of ice floes and ice failure between numerical simulations and ice tank tests on managed ice condition. The authors have been developing a DEM simulation by using the Bullet since 2017 and shown some results such as the size effect of ice floes and the overestimated peak load measured in an ice tank test conducted in 2017 at the ice model basin of National Maritime Research Institute (Hasegawa, et al., 2018; 2019). In this simulation, ice failure, which was observed in the test, was not taken into account.

In this study, a breakable ice element consisting of small rigid body with a fixed joint function of the physics engine is introduced to our numerical simulation method in order to represent ice failure. This paper first briefly describes the experiments conducted in 2017 and then the numerical simulation method. To clarify the effect of ice failure, the simulation and the experiment results are compared in two sizes of ice floe.

EXPERIMENTS

This section briefly describes the experiments conducted in 2017 at the ice model basin of National Maritime Research Institute. The water contains Propylene Glycol as a dopant and model ice with columnar crystal structure is produced. Details are given in Hasegawa et al (2018). Figure 1 and Table 1 show the section view of the ice model basin and specifications, respectively. The structure model has an inverted conical shape with the principal dimensions shown in Figure 2 and Table 2. The structure model is fixed to a 6-component load cell installed on the towing carriage, and load exerted on the model is measured. The towing speed is constant at 0.07 m/s, and the structure model collides with stationary ice floes. Figure 3 shows the initial arrangements of ice floes. 0.3 m- (Figure 3(a)) and 0.6 m-square shaped (Figure 3(b)) ice floes are used. Target ice thickness and density are 0.03 m and 930 kg/m^3, respectively. For each ice floe size, the test is conducted with ice concentration (IC) of 75%. A part of a mother ice sheet is left on the side walls of the ice model basin so that ice floes do not interact with the tank walls. Bending strength and elastic modulus of the model ice are measured by cantilever-beam tests and a plate deflection method, respectively.

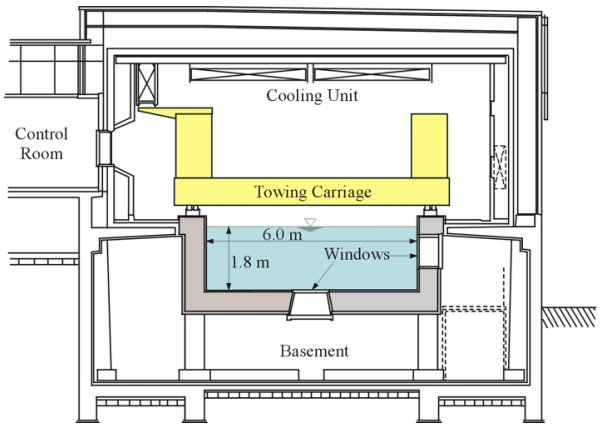

Figure 1. Section view of ice model basin

Table 1. Specifications of ice model basin

ITEM	UNIT	VALUE
Length	m	35.0
Breadth	m	6.0
Water depth	m	1.8
Freezing rate	mm/h	2~3

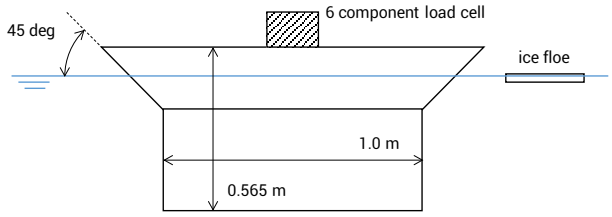

Figure 2. Cross-sectional view of the conical structure model

Table 2. Principal dimensions of conical structure

ITEM	UNIT	VALUE
Breadth maximum	m	1.472
Breadth water line	m	1.228
Draft	m	0.443
Depth molded	m	0.565

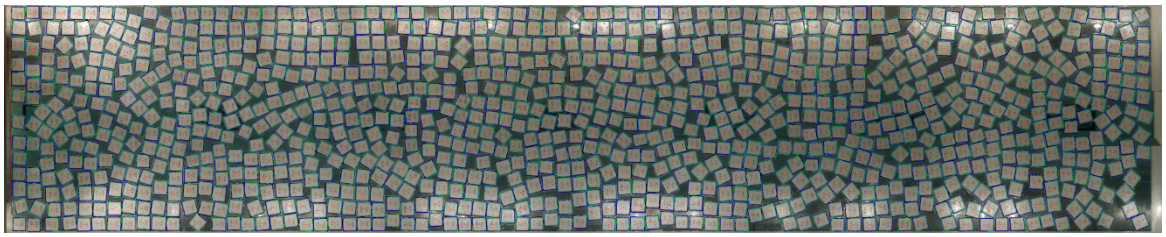

(a) Smaller ice floes with a channel length of about 24 m

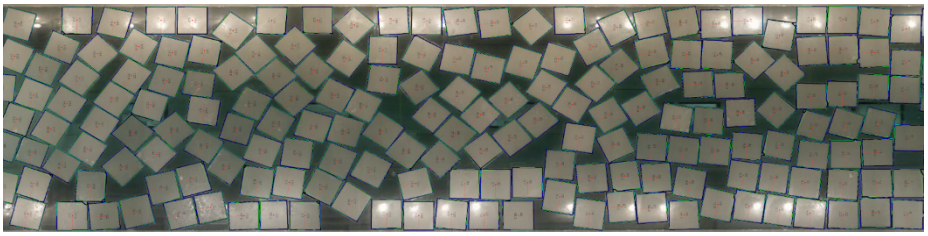

(b) Larger ice floes with a channel length of about 20 m

Figure 3. Top view of initial arrangement of ice floes in the experiments for IC of 75% and a channel width of 4.8 m. The structure model moves from left to right on this image.

NUMERICAL SIMULATION

Non-smooth Discrete Element Method

Discrete Element Methods (DEMs) are often used for multiple body problems in many fields. There are roughly two approaches in DEMs, one is a smooth approach (Cundall and Strack, 1979) in which an interaction force is applied according to the penetration amount of objects by taking into account of the viscoelasticity nature of contact. The other is a non-smooth approach (Jean, 1999) in which objects are assumed to be rigid in general. Collision and stick-slip friction transition are considered as instantaneous events according to a given contact law. The authors compared the results by non-smooth DEM simulation with the experimental results in case of single ice floe-structure interaction and showed that the impact load can be qualitatively reproduced well (Hasegawa, et al., 2018). The projected Gauss-Seidel method (Catto, 2005) is used for solving the constraint forces by satisfying the constraint condition at each time step. To implement the non-smooth DEM, Bullet Physics Library version 8.26 developed by Coumans (2017) is used in this study.

Simulation design

We numerically simulate the structure-multiple ice floes interaction corresponding to the experiments. Table 3 summarizes the simulation conditions. The bending strength and the elastic modulus are obtained from the strength tests in the experiment. The compressive strength and the shear strength are set to be 4 times and twice as large as the bending strength

respectively (Schwarz and Weeks, 1977). For the coefficient of friction between ice and ice, simulations are carried out with three parameters with reference to the experiments by Repetto-Llamazares et al. (2011), and Sukhorukov and Løset (2013). According to their reports, the friction coefficient tends to increase as the sliding speed and the normal force are reduced. We conducted the friction experiments and confirmed that f_{ii} was about 0.5. Therefore, parametric study with f_{ii} of 0.3, 0.5, 0.7 and f_{is} of 0.1, 0.2, 0.3 is conducted in this paper.
The coordinate system and the initial arrangement of ice floes are shown in Figure 4. The shaded area indicates a stationary ice sheet adjacent to the tank walls. The initial arrangements of ice floes are reproduced from those of the experiment shown in Figure 3 by image segmentation with the watershed algorithm (Meyer, 1992). The numerical model of the structure advances at a constant speed of 0.07 m/s from $x = 2\ m$ in the surge direction, and collides with ice floes arranged in the range of $x \geq 6\ m$ and $-2.4 \leq z \leq 2.4\ m$. The structure model moves only in the surge direction, and the ice floes can move in 6 degrees of freedom. In the present simulation, hydrodynamic force is applied to ice floes on the assumption of a simple flow around the structure. More detailed description of this numerical simulation is in Hasegawa et al (2018 and 2019).

Table 3. Simulation conditions

ITEM	SYMBOL	UNIT	VALUE
Ice concentration	IC	%	75
Ice floe			
length × breadth	$L_i \times B_i$	m	0.3 × 0.3 / 0.6 × 0.6
thickness	T_i	m	0.033
density	ρ_i	kg/m^3	930.0
bending strength	σ_b	kPa	36.4
compressive strength	σ_c	kPa	145.6
shear strength	σ_s	kPa	72.8
elastic modulus	E	MPa	60.0
Water density	ρ_w	kg/m^3	1000.0
Structure speed	V	m/s	0.07
Coef. of restitution			
ice-ice	e_{ii}	-	0.0
ice-structure	e_{is}		0.0
Coef. of friction			
ice-ice	f_{ii}	-	0.3 / 0.5 / 0.7
ice-structure	f_{is}	-	0.1 / 0.2 / 0.3
Timestep	Δt	sec	0.02

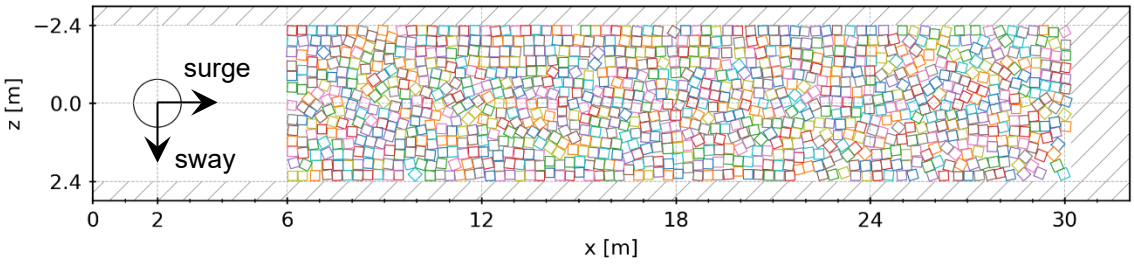

Figure 4. Initial arrangement of ice floes reproducing Figure 3(a) in the numerical simulation. The structure moves from $x = 2\ m$ in the surge direction.

Breakable Ice Element

The image of the breakable ice element adopted in this paper is shown in Figure 5. An ice floe is divided into small rigid elements which are connected to each other through a fixed joint function of the physics engine. Ice failure is simply represented by disconnecting the joint when the constraint force exerted on the joint exceeds a threshold based on ice strength. This approach is often used for a collapse simulation of a building which is necessary to track a large number of fragments, e.g. in Hamano et al. (2016) and in Walter and Kostack (2015).

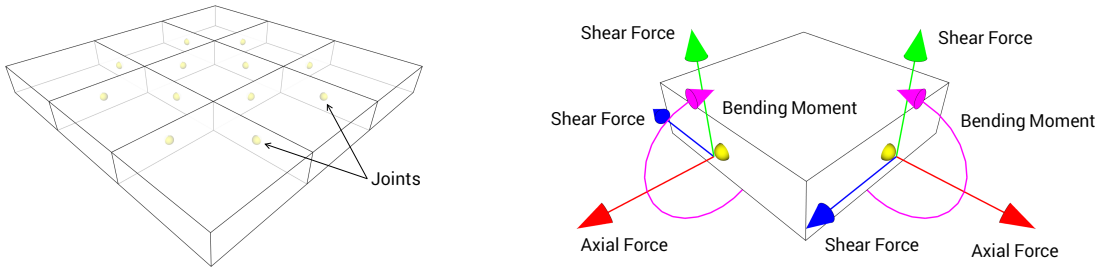

(a) Ice floe consisting of small elements (b) Forces dealt with at joints

Figure 5. Image of breakable ice element

In this method, the shape of a broken ice floe depends on the shape of the breakable ice element. Elements with a square shape are used in this paper. Although this results in the simple failure pattern, the movement and hydrodynamic force on the broken ice floe can be calculated more simply and correctly than complicated shapes. Ice failure occurs if one of the following conditions are satisfied at each joint:

$$\lambda_c > \varepsilon_c = L_e T_e \sigma_c \qquad \text{(compression failure)} \qquad (1)$$

$$\lambda_s > \varepsilon_s = L_e T_e \sigma_s \qquad \text{(shear failure)} \qquad (2)$$

$$\lambda_b > \varepsilon_b = \frac{L_e T_e^2}{6} \sigma_b \qquad \text{(bending failure)} \qquad (3)$$

where λ is the constraint force/moment, ε is the threshold, L_e is the length of the element, and T_e is the thickness of the element. Bullet physics engine uses parameters of the constraint force mixing (Σ) and the error reduction parameter (Γ) to permit Baumgarte stabilization method (Baumgarte, 1972) which reduce constraint error efficiently. Σ and Γ are expressed as

$$\Sigma = \frac{1}{\Delta t K + D} \qquad (4)$$

$$\Gamma = \frac{\Delta t K}{\Delta t K + D} \qquad (5)$$

where K is the spring constant and D is the damping constant. Constraint forces can be reinterpreted as arising from the same effect as a spring-damper system (Li, et al., 2018), which means that elements are connected by a spring and a damper. The value of Γ is set to 0.8 within the recommended range in Bullet. It is reported that Σ greatly contributes to the hardness of constraints. Therefore, the numerical simulation is conducted in the situation of the plate deflection test and the simulated elastic modulus is compared with the experiment data. The results are shown in Figure 6 when the sizes of an ice sheet (L_i) are 5.4 and 2.7 m and the element sizes (L_e) are 0.10, 0.15 and 0.20 m. From the results, it is found that the elastic modulus is determined by the element size and the value of Σ. In this study, we use two kinds of elements: a size of 0.15 m with Σ of 10^{-10} and a size of 0.20 m with Σ of 0.016.

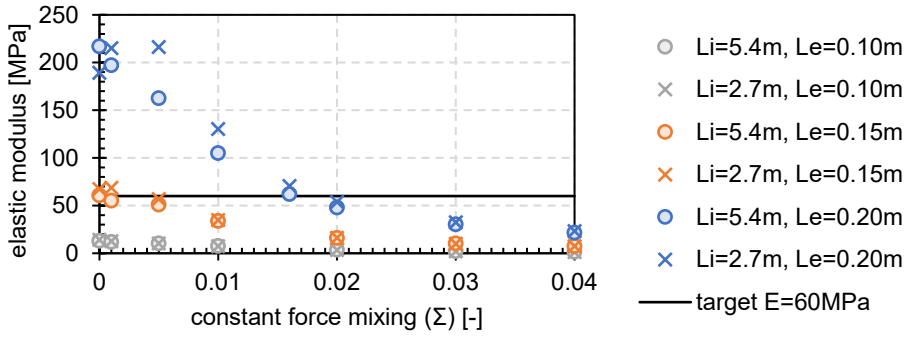

Figure 6. Influence of Σ on the elastic modulus of the numerical ice floe

In addition, a cantilever-beam test is conducted in the numerical simulation to confirm whether ice failure is properly reproduced in this model. A beam is formed by connecting the elements and one end of the elements is fixed. The other end of the elements is pushed down at a constant speed until ice failure occurs. The time curves of reaction force (P_c) during pushing down are shown in Figure 7(a). The peak load indicates the occurrence of bending failure, and the remaining load after that is the buoyancy of the fragment. Figure 6(b) shows the bending stress (σ') at the failure location calculated from the reaction force shown in Figure 6(a) by the following equation:

$$\sigma' = \frac{6(P_c - P_b)l}{L_e T_e^2} \tag{6}$$

where l is the distance between the failure location and the pushed down point, and P_b is the buoyancy of the beam. The failure occurs well at a value close to the measured bending strength. Since it is thought that accurate P_b of the inclined beam during the test is not obtained by pushing down the fragment, the maximum bending stress becomes larger than it. Thus, the influence on this simulation is considered to be small.

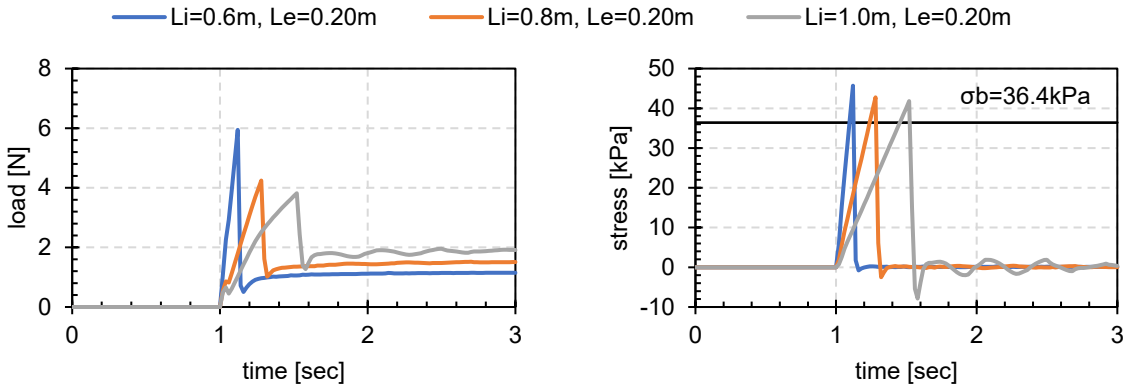

(a) Reaction force (b) Bending stress at the failure location

Figure 7. Cantilever-beam test for the element size of 0.20 m

RESULTS AND DISCUSSIONS

Smaller Ice Floes

Figure 8 shows the result of statistical analysis for the smaller ice floes condition (Figures 3(a) and 4). In this case, almost no ice failure occurs in the experiment. This is because the ice floe size of 0.30 m is smaller than the characteristic length of about 0.35 m obtained from the ice

properties such as the elastic modulus and the ice thickness shown in Table 3. Thus, we numerically simulate without breakable ice elements. As f_{is} and f_{ii} increases, the average load also basically increases. However, the average load for f_{is} of 0.3 and f_{ii} of 0.5 becomes largest because managed ice condition is a very random phenomenon due to interaction with a large number of ice floes. Although the maximum load shows a large variation among the conditions, it can be seen that the maximum load becomes larger as f_{is} increases. Both the average load and maximum load become close to the experimental results when f_{is} is between 0.2 and 0.3.

The time history of ice load for f_{ii} of 0.5 is shown in Figure 9. Each result is shifted in time so that the time of the first collision with an ice floe is 0 *sec*. The results of the experiment and the simulations do not include hydrodynamic resistance of the structure. The statistical analysis is carried out in the time range shown in Figure 9 (after the structure has advanced the twice length of that in the ice channel). Peak loads in the simulation appear at about 4 *sec* intervals. This interval is approximately equal to the time the structure passes through the size of one ice floe.

Figure 10 shows the front view of the trajectory of ice floes obtained by simulations. Figure 10(a) shows the trajectory of ice floes obtained in the previous test (Hasegawa et al., 2019). In this test, f_{is} and f_{ii} are 0.1 and the calculated average ice load underestimated the experiment by about 10 *N*. Figure 10(b) shows the trajectory under the condition of the average ice load close to the experimental result in the present paper. The increase in f_{is} and f_{ii} results not only in increased ice load but also in the behavior of ice floes being submerged to a greater depth.

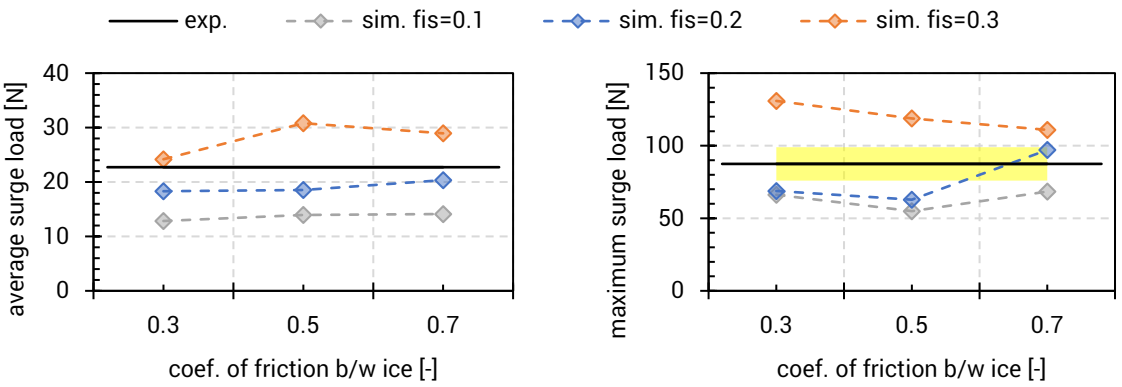

(a) Average ice load in surge direction

(b) Max. ice load in surge direction. Yellow area shows standard deviation in open water.

Figure 8. Simulation and experimental results for smaller ice floes

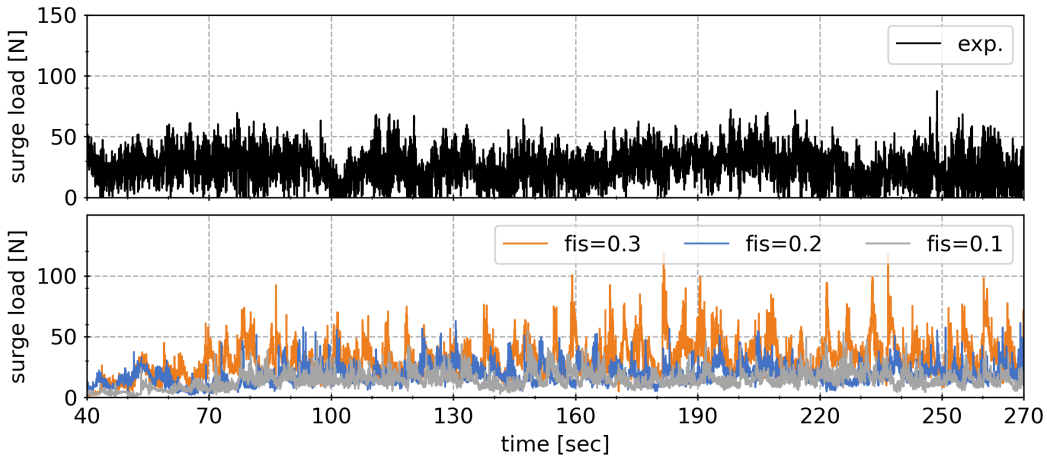

Figure 9. Time history of ice load in surge direction for f_{ii} of 0.5 and smaller ice floes

Such behavior of ice floes and accumulation of multiple ice floes in front of the model are reproduced well in the numerical simulation as shown in Figure 11. From these results, it is found that ice load and behavior of ice floes can be qualitatively reproduced well in case that global ice failure such as bending and splitting does not occur.

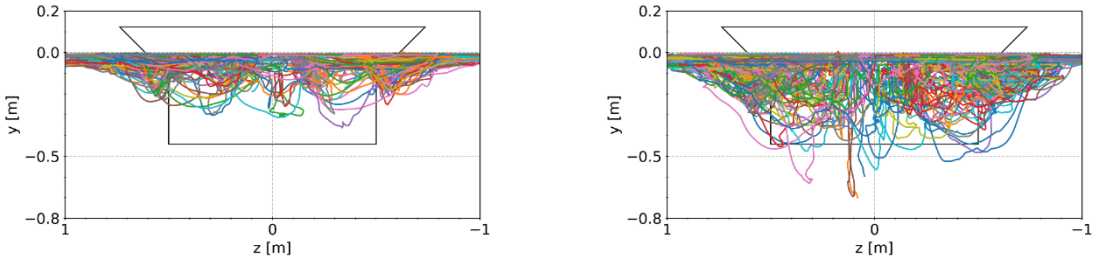

(a) For f_{is} of 0.1 and f_{ii} of 0.1 (Hasegawa et al., 2019)

(b) For f_{is} of 0.3 and f_{ii} of 0.3

Figure 10. Front view of ice floes trajectory. The vertical and horizontal axes indicate the heave and sway directions, respectively.

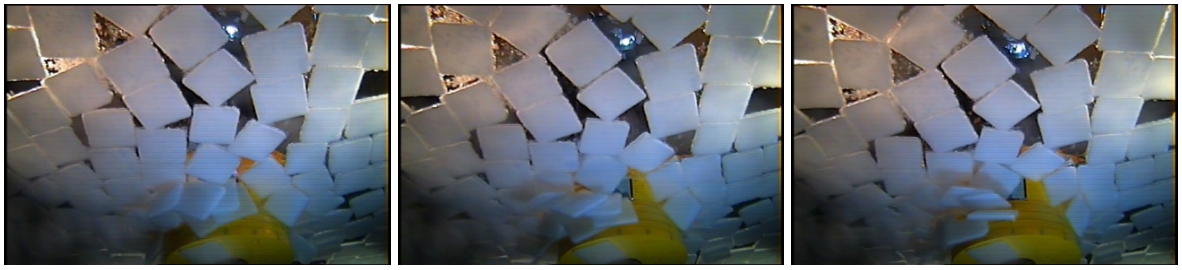

(a) In the experiment at 212, 214, 261 *sec* (Hasegawa et al., 2019)

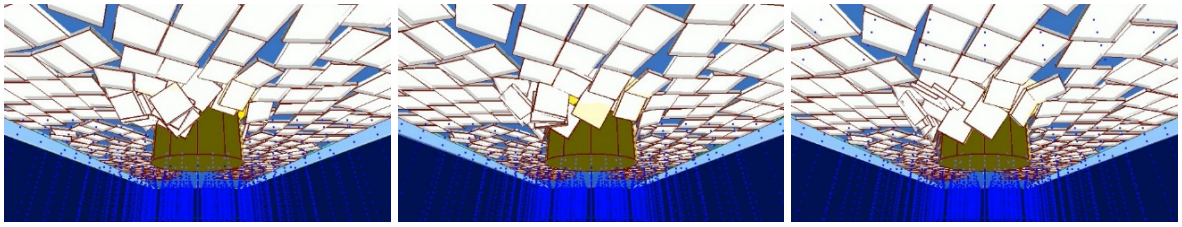

(b) In the simulation for f_{is} of 0.3 and f_{ii} of 0.3 at 100, 102, 104 sec

Figure 11. State of ice floes accumulating in front of the structure

Larger Ice Floes without Ice Failure in Numerical Simulation

Figure 12 shows the result of statistical analysis for the larger ice floes condition (Figure 3(b)). In this case, ice failure occurs in the experiment. In this section, however, we numerically simulate without breakable ice elements to clarify the effect of ice failure. The average and maximum load of the experimental result are increased by about 50% and 100%, respectively, compared to those for the smaller ice floes (Figure 8). The average load becomes close to the experimental results when f_{is} is between 0.2 and 0.3. This agrees with the result in the case of the smaller ice floes (Figure 8(a)). On the other hand, the maximum loads of the simulation results are extremely overestimated as compared with that of the experimental result.

The time history of ice load for f_{ii} of 0.5 is shown in Figure 13. It can be seen that an ice load of more than 300 *N*, which is about twice that of the experimental result, is generated several times in each condition of f_{is}. The state of ice floes around the structure in the simulation is shown in Figure 14 when such a very large load is generated. The figure shows that movement

of the ice floes contacted with the structure is constrained by surrounding ice floes (Figure 14(a)) and ice floes stick in the whole channel (Figure 14(b)). At that time, a load network is formed to the sides and end of channel, resulting in a very large load.

In the experiment, ice failure occurs as shown in Figure15 when ice loads exceed ice strength, and the fragments create some gaps. Such gaps make ice floes more mobile and prevent the formation of a load network, resulting in a decrease in ice loads. Thus, peak load of the simulation results is estimated much higher than that of the experimental result. Global ice failure is regarded as relaxation phenomenon for ice load exerted on the structure.

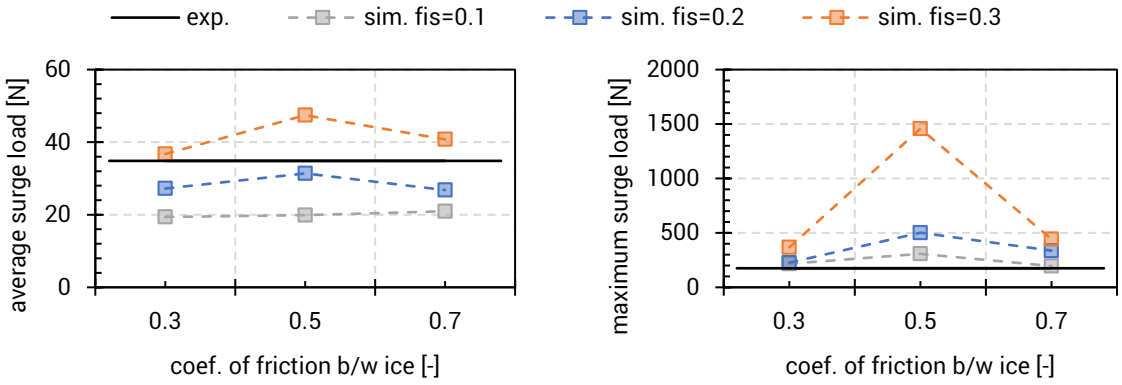

(a) Average ice load in surge direction (b) Max. ice load in surge direction.

Figure 12. Simulation and experimental results for larger ice floes without ice failure in numerical simulation

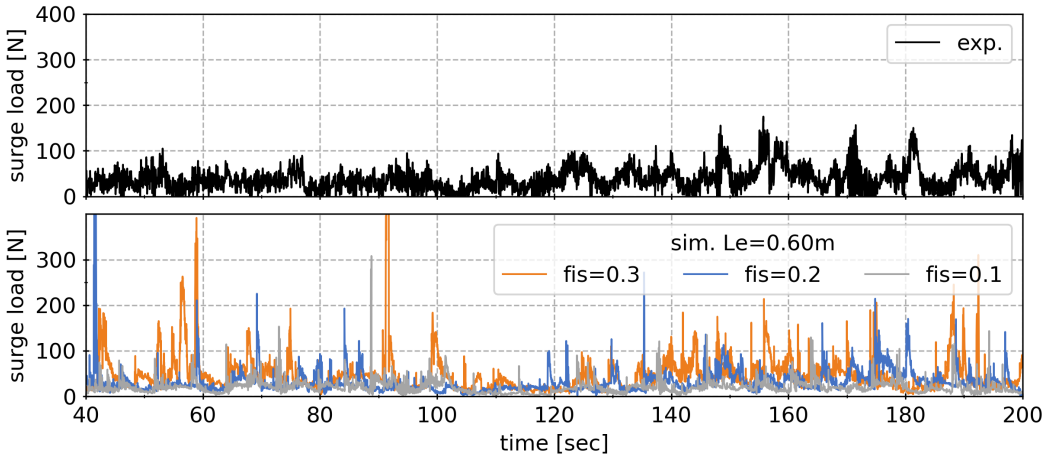

Figure 13. Time history of ice load in surge direction for f_{ii} of 0.5 and larger ice floes

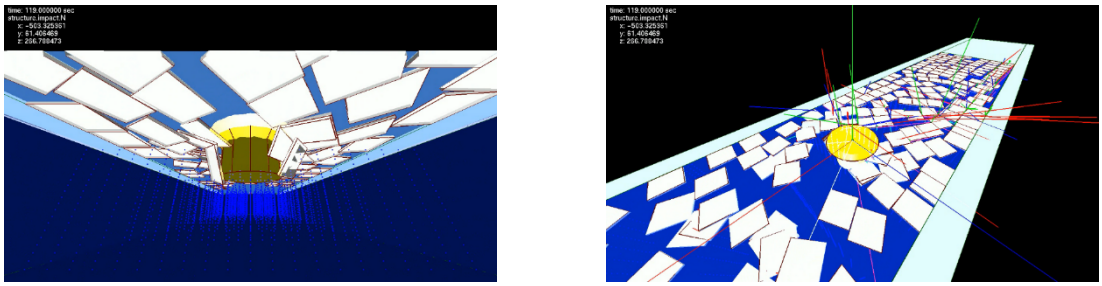

(a) Front view (b) General view

Figure 14. State of ice floes around the structure in the numerical simulation for the larger ice floes with f_{is} of 0.3 and f_{ii} of 0.5 at 90 *sec*

(a) Bending failure b/w ice-structure

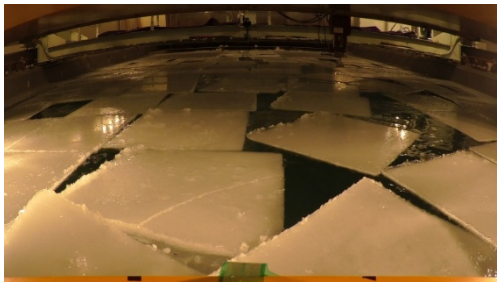

(b) Bending failure b/w ice-ice

Figure 15. State of ice floes around the structure in the experiment for the larger ice floes

Larger Ice Floes with Ice Failure in Numerical Simulation

Figure 16 shows the result of statistical analysis for the larger ice floes condition (Figure 3(b)) with breakable ice elements in the simulation. The experimental results are the same as the previous section. The average load shows a similar trend to that of the simulation result for the larger ice floes without breakable ice elements (Figure 12(a)). It can be seen that the influence of the element size on the average load is small. The maximum load, which is extremely large in the previous section, decrease to the order of the experimental result by taking ice failure into account. The maximum load also becomes close to the experimental results when f_{is} is between 0.2 and 0.3. It shows a similar trend to the result in the case of the smaller ice floes (Figure 8(b)). From the results for the two sizes of ice floe, we find that the numerical simulations using breakable ice elements qualitatively reproduce well the experiments and a value of 0.2 to 0.3 is appropriate for f_{is} in terms of ice loads.

The time history of ice load for f_{ii} of 0.5 is shown in Figure 17. It can be seen that an ice load of about 300 N, which is about twice that of the experimental result, is generated only once for f_{is} of 0.3, f_{ii} of 0.5 and L_e of 0.20 m. Ice loads qualitatively reproduce the experimental result well except at the time when the peak load of about 300 N occurred.

In the experiment, it was observed that most frequent mode of ice failure is bending. Ice floes are often broken by bending while sliding on the slope of the structure after collision with the structure as shown in Figure 15(a). In the present simulation, all the ice failure is by bending. However, the state of ice failure is different depending on f_{ii}. For f_{ii} of 0.3, it is frequently

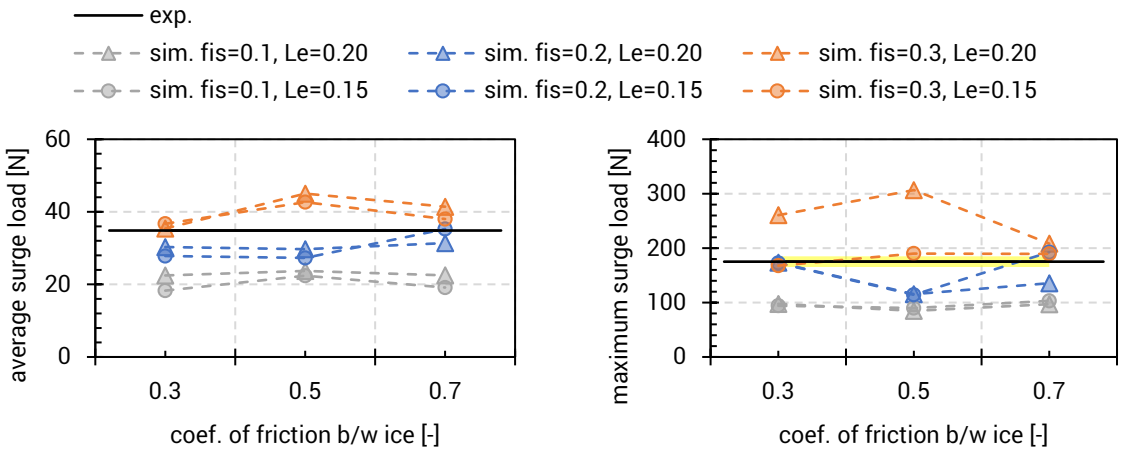

(a) Average ice load in surge direction

(b) Max. ice load in surge direction. Yellow area shows standard deviation in open water.

Figure 16. Simulation and experimental results for larger ice floes with ice failure in numerical simulation

observed that approaching ice floe presses submerged ice floe against the structure and then bending failure of the submerged ice floe occurs (Figure 18(a)). For f_{ii} of 0.7, ice floes are sometimes broken by bending while sliding on the slope as was observed in the experiment (Figure 18(b)). This may be because the friction force between ice floes prevents an ice floe from rotating, resulting in an increase in bending moment.

Since breakable ice elements with a square shape are used in this study, ice failure is represented only in the form of squares or rectangles. By using a hexagon as a shape of the element, it is expected that ice failure can be represented in a form close to a shape having a curved surface.

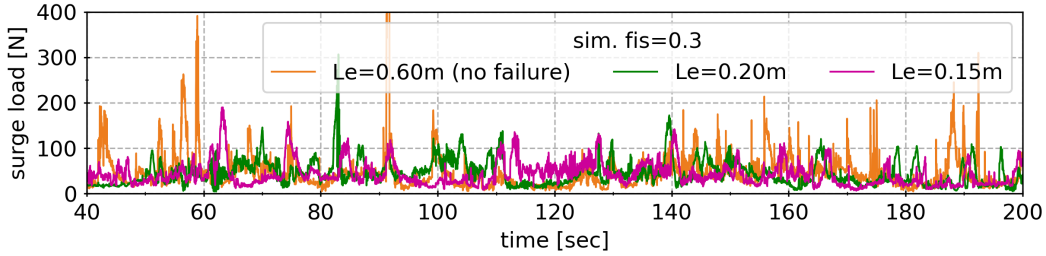

Figure 17. Time history of ice load in surge direction for f_{ii} of 0.5

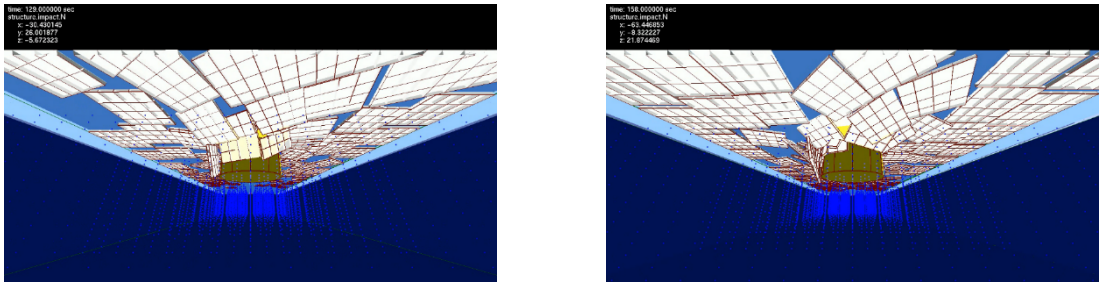

(a) For f_{ii} of 0.3 (b) For f_{ii} of 0.7

Figure 18. State of ice failure in the numerical simulation for f_{is} of 0.3 and L_e of 0.15 m

CONCLUSIONS

We numerically simulated the structure-multiple ice floes interaction by a non-smooth discrete element method. In this study, a breakable ice element consisting of small square rigid body with a fixed joint function of the physics engine of Bullet is introduced to our simulation method in order to represent ice failure of managed ice floes. To clarify the effect of the ice failure, we have compared the simulation results with the experiments, which conducted in the ice model basin of National Maritime Research Institute, in two sizes of ice floes

For smaller ice floes, ice failure was almost not observed in the experiment. Thus, ice load and behavior of ice floes can be qualitatively reproduced well even without breakable ice elements when f_{is} is between 0.2 and 0.3. For larger ice floes, on the other hand, ice failure was frequently observed in the experiment. Although the results of the simulation without breakable ice elements show extremely higher peak loads than that of the experiment, the breakable ice elements reasonably reduce peak loads to the experimental results. Furthermore, we find that the state of ice failure is different depending on f_{ii}. The state of ice failure similar to the experiment was sometimes observed for larger f_{ii} of 0.7.

ACKNOWLEDGEMENTS

This work was supported by JSPS KAKENHI Grant Number JP17K14890.

REFERENCES

Baumgarte, J., 1972. Stabilization of constraints and integrals of motion in dynamical systems, *Computer Methods in Applied Mechanics and Engineering*, 1(1), pp.1-16.

Catto, E., 2005. Iterative Dynamics with Temporal Coherence, *Game Developer Conference*.

Coumans, E., 2017. Bullet Physics Library version 2.86, [Online] Available at: http://bulletphysics.org/ [Accessed 1 December 2017].

Cundall, P.A. & Strack, O.D.L., 1979. A discrete numerical model for granular assemblies, *Geotechnique*, 29(1), pp.47-65.

Jean, M., 1999. The non-smooth contact dynamics method, *Computer Methods in Applied Mechanics and Engineering*, 177, pp.235-257.

Dudal, A., Septseault, C., Beal, P.A., & Yaouanq, S.L., 2015. A NEW ARCTIC PLATFORM DESIGN TOOL FOR SIMULATING ICE-STRUCTURE INTERACTION, *Proceedings of the 23rd International Conference on Port and Ocean Engineering under Arctic Conditions.*

Gautier, D.L. & Moore, T.E., 2017. Introduction to the 2008 Circum-Arctic Resource Appraisal (CARA) Professional Paper. *The 2008 Circum-Arctic Resource Appraisal: U.S. Geological Survey Professional Paper*, 1824, 9p.

Hamano, T., Onosato, M., & Tanaka, F., 2016. *Performance Comparison of Physics Engines to Accelerate House-Collapsing Simulations*, Proceedings of the IEEE International Symposium on Safety, Security and Rescue Robotics, pp.358-363.

Hasegawa, K., Uto, S., Shimoda, H., Wako, D., & Matsuzawa, T., 2018. Numerical and Experimental Investigations of Managed Ice Loads acting on Fixed Conical Structure, *Proc. of the 28th International Ocean and Polar Engineering Conference*, 28, pp.1672-1678.

Hasegawa, K., Uto, S., Shimoda, H., Wako, D., & Matsuzawa, T., 2019. Influence of Initial Arrangement of Ice Floes on Ice Loads in Non-smooth Discrete Element Method Simulation, *Proc. of the 34th International Symposium on Okhotsk Sea and Polar Oceans,* 34, pp.126-129.

Konno, A., Nakane, A., & Kanamori, S., 2013. VALIDATION OF NUMERICAL ESTIMATION OF BRASH ICE CHANNEL RESISTANCE WITH MODEL TEST, *Proceedings of the 22nd International Conference on Port and Ocean Engineering under Arctic Conditions*.

Li, X., Andrews, S., Jones, B., & Bargteil, A., 2018. Energized Rigid Body Fracture, *Proceedings of the ACM on Computer Graphics and Interactive Techniques*, 1(1), 9p.

Lubbad, R. & Løset S., 2015. Time Domain Analysis of Floe Ice Interactions with Floating Structures, *Proceedings of the Arctic Technology Conference*.

Polojärvi, A., Tuhkuri, J., & Korkalo, O., 2012. Comparison and analysis of experimental and virtual laboratory scale punch through tests, *Cold Regions Science and Tech.*, 81, pp.11-25.

Repetto-Llamazares A. H.V., Høyland K.V., & Kim, E., 2011. Experimental studies on shear failure of freeze-bonds in saline ice: Part II: Ice-Ice friction after failure and failure energy, *Cold Regions Science and Technology,* 65, pp.298-307.

Schwarz, J. & Weeks, W.F., 1977. ENGINEERING PROPERTIES OF SEA ICE, *Journal of Glaciology*, 19(81), pp.499-531.

Sukhorukov, S. & Løset S., 2013. Friction of sea ice on sea ice, *Cold Regions Science and Technology*, 94, pp.1-12.

Walter, O. & Kostack, K., 2015. Bullet Constraints Builder for collapse simulation, [Online] Available at: https://www.blender.org/conference/2015/presentations/190 [Accessed 1 December 2018].